ISSN 0036-0244, Russian Journal of Physical Chemistry A, 2023, Vol. 97, No. 10, pp. 2241–2257. © Pleiades Publishing, Ltd., 2023.

PHYSICAL CHEMISTRY OF NANOCLUSTERS, SUPRAMOLECULAR STRUCTURES, AND NANOMATERIALS

Coating of Al–X (X = Mg, Ga, Si) Alloys Nanosurface with Organic Corrosion Inhibitors Using TD-DFT Approach: Intra-Atomic and Interatomic Investigation through Langmuir Adsorption Study

Fatemeh Mollaamin[a,*] and Majid Monajjemi[b]

[a] *Department of Food Engineering, Faculty of Engineering and Architecture, Kastamonu University, Kastamonu, Turkey*

[b] *Department of Chemical Engineering, Central Tehran Branch, Islamic Azad University, Tehran, Iran*

** e-mail: smollaamin@gmail.com*

Received September 23, 2022; revised November 30, 2022; accepted March 14, 2023

Abstract—The adsorption analysis of some organic inhibitors consisting of benzotriazole, 8-hydroxyquinoline, 2-mercaptobenzothiazole onto aluminum alloy surface based on optimized coordination of binding on the Al–X (Mg, Ga, Si) surface has been accomplished. In this work, the ONIOM approach has been performed with a three-layered level of high level of DFT method using EPR-III, 6-31+G(*d*,*p*) and LANL2DZ basis sets by the physico-chemical software of Gaussian 16 revision C.01 program, a medium semi-active part that includes important electronic contributions, and a low level part that has been handled using MM2 force field approaches. The physico-chemical properties of adsorption -surface complexes are one of the principal parameters for determining and choosing the Langmuir adsorption through IR, NMR, UV–Vis, HOMO/LUMO and charge distribution results. Comparing to ΔG°_{ads} amounts approved a good agreement among computed results, as well as the correctness of the selected isotherm for the adsorption process of benzotriazole → Al–Mg, benzotriazole → Al–Ga, benzotriazole → Al–Si, 8-hydroxyquinoline → Al–Mg, 8-hydroxyquinoline → Al–Ga, 8-hydroxyquinoline → Al–Si, 2-mercaptobenzothiazole, 2-mercaptobenzothiazole → Al–Mg, 2-mercaptobenzothiazole → Al–Ga, and 2-mercaptobenzothiazole → Al–Si. Nuclear magnetic resonance has certainly has focused on the aluminum shielding in the intra-atomic interaction with magnesium, gallium and silicon and simultaneously interatomic interaction with other atoms in organic inhibitors through variety of high, medium and low layers of ONIOM method. Al–Si with highest fluctuation in the shielding tensors of NMR spectrum generated by intra-atomic interaction leads us to the most influence in the neighbor atoms generated by interatomic reaction. Moreover, based on the computed amounts of UV–Vis spectra for benzotriazole, 8-hydroxyquinoline and 2-mercaptobenzothiazole adsorb on the Al(111)-alloy surface, there are maximum adsorption bands between 200–280 nm for benzotriazole, 225–350 nm for 8-hydroxyquinoline and 210–280 nm for 2-mercaptobenzothiazole, respectively; and maximum adsorption bands for benzotriazole, 8-hydroxyquinoline, and 2-mercaptobenzothiazole has observed around 230, 300, and 240 nm, respectively.

Keywords: Langmuir adsorption, benzotriazole, 8-hydroxyquinoline, 2-mercaptobenzothiazole, Al–Mg, Al–Ga, Al–Si, ONIOM, CAM-DFT, NMR, IR, UV–Vis, HOMO, LUMO

DOI: 10.1134/S0036024423100096

1. INTRODUCTION

An aluminum alloy is an alloy in which Al is the major metal. However, the special alloying elements are Cu, Mg, Mn, Si, Sn, Ni, and Zn. Light weight or corrosion resistance of aluminum alloys make them suitable in engineering structures and components.

Aluminum–silicon (Al–Si) is one of the most important aluminum alloys with high amounts of silicon in casting and has a large limitation of usages in the aerospace and automotive industries through a best combination of mechanical properties, as well as good wear resistivity and corrosion resistance [1–3].

Si element in Al–Si based cast alloys impacts tensile properties at both room and high temperature, but its role becomes more important in lack of alloy elements such as Mg, Fe, and Cu [4].

Some elements like Cu and Mg added to Al alloys ameliorate the mechanical attributes and conduct the alloy to reply the heat dealing. The existence of magnesium also increases resistance and reduces the rate of strength loss at high temperature in the alloys. Alu-

minum-magnesium (Al–Mg) alloys are lighter than other aluminum alloys and much less flammable than other alloys consisting of high amounts of magnesium. The magnificent enhancement in resistance at elevated temperature was accomplished after solution treatment through activating settlement becoming hard through Mg possessing phases.

Most inhibitors deduce or prohibit corrosion of aluminum by either cathode or anodic reactions. Usage of chromates (which extinguish the anodic reactions with coatings as the inhibitions for aluminum sheets) has reduced because of toxicity. Other compounds like phosphates, silicates, nitrates, nitrites, benzoates, *N*-heterocyclic structures can influence the cathodic reactions in aqueous environment.

Among the various methods that minimize corrosion of metal surface, its inhibition by organic molecules is one of the most applicable methods because of its stability and low cost [5–9]. There are many researches that have been dedicated to the application of efficient heterocyclic and heteroatomic including organic compounds that ameliorate the anticorrosion attributes of metal surfaces and alloys. The existence of heteroatoms containing O, S, N, P atoms, aromatic rings and multiple bonds with π-electrons in these inhibitors help extensively to the formation of inactive blocks on metal surface and alloys, so closing the active sites of corrosion [10–16].

Aluminum–gallium (Al–Ga) which is a degenerate alloy is obtained from liquid gallium diffusing the crystal structure of Ga metal. This alloy is so much fragile that is broken under a little pressure. Al–Ga alloy is also chemically more fragile, because it prevents Al from forming a protective oxide layer. This element and its alloys are usually employed experimental fluids for modeling both liquid and solid dynamics in planetary cores. Al–Ga is able to react with H_2O molecules to produce Al oxide, Ga metal, and hydrogen gas. Al reacts in air to generate an inactive layer of aluminum oxide and it doesn't react with water. Aluminum-Gallium alloy can form Al nanoparticles for the hydrogen creating reaction [17].

Based on some researches, benzotriazole, 8-hydroxyquinoline, and 2-mercaptobenzothiazole are organic cyclic inhibitors for metal, semi-metals or non-metals surfaces and theirs alloys by preventing undesirable surface reactions. It is obvious that a passive layer, containing a complex between surface and these inhibitors, is generated when surface is immersed in a solution consisting of benzotriazole, 8-hydroxyquinoline and 2-mercaptobenzothiazole. The passive layer is insoluble in aqueous and many organic solutions. There is a positive connection between the thickness of the passive layer and the efficiency of preventing corrosion [18–20].

In present work, we have investigated on adding some alloying elements of Mg, Ga, and Si to Al surface which have been coated with organic compounds of benzotriazole, 8-hydroxyquinoline, 2-mercaptobenzothiazole as the corrosion inhibitors of Al alloys.

2. THEORY, MATERIALS AND METHODS

2.1. Corrosion Heterocyclic Inhibitors

Recently, some researches have investigated that organic compounds can be employed as corrosion inhibitors for Al and its alloys, because they consist of several heteroatoms (N, S, O, and P) which act as active adsorption centers. In this research, we discuss the use of organic compounds of benzotriazole, 8-hydroxyquinoline, 2-mercaptobenzothiazole as corrosion inhibitors for Al(111)-alloys [21].

In this research, it has been attributed the inhibiting effect of the benzotriazole, 8-hydroxyquinoline, 2-mercaptobenzothiazole to the adsorption of a stable complex formed on the aluminum(111)-alloys of Al–Mg, Al–Ga, and Al–Si surfaces. The reactivity and adsorption behavior of the three mentioned inhibitors on the Al(111)-alloys were analyzed, and the interaction mechanism of inhibitors → Al(111)-alloys was revealed to provide a theoretical reference and guidance for electrodeposition of aluminum-alloy in the aqueous medium. For each of the crystal systems, there is, in principle, an infinite number of the possible lattice that can be exposed. The interval of the closest approach of atoms is 0.28630 nm (Scheme 1). Scheme 1 has shown the fragments (active site) of the interaction between inhibitors of benzotriazole, 8-hydroxyquinoline, 2-mercaptobenzothiazole and Al(111)-alloys including Al–Mg, Al–Ga, and Al–Si surfaces. Each fragment consists of 12 atoms including 7 atoms of aluminum, 5 atoms of magnesium or gallium or silicon.

2.2. Model of Langmuir Adsorption

The study involving the influence of the organic inhibitors in solution and the nature of the corrosive aluminum alloys on the adsorption bond strength yield information about the mechanism of interaction of the inhibitor with the Al(111) alloys-surface, which in turn Langmuir adsorption isotherms provide excellently. The Langmuir isotherm is widely used in the identification of inhibitor adsorption status specification [22, 23].

The adsorption of benzotriazole, 8-hydroxyquinoline, 2-mercaptobenzothiazole as corrosion inhibitors on the aluminum alloys surface including Al–Mg, Al–Ga, and Al–Si in NaCl solution was assigned by the most suitable Langmuir isotherm, which exhibits the chemisorptive nature of the bond between the inhibitor molecules and the Al(111)-alloys, the equilibrium distribution of ions of the adsorbing com-

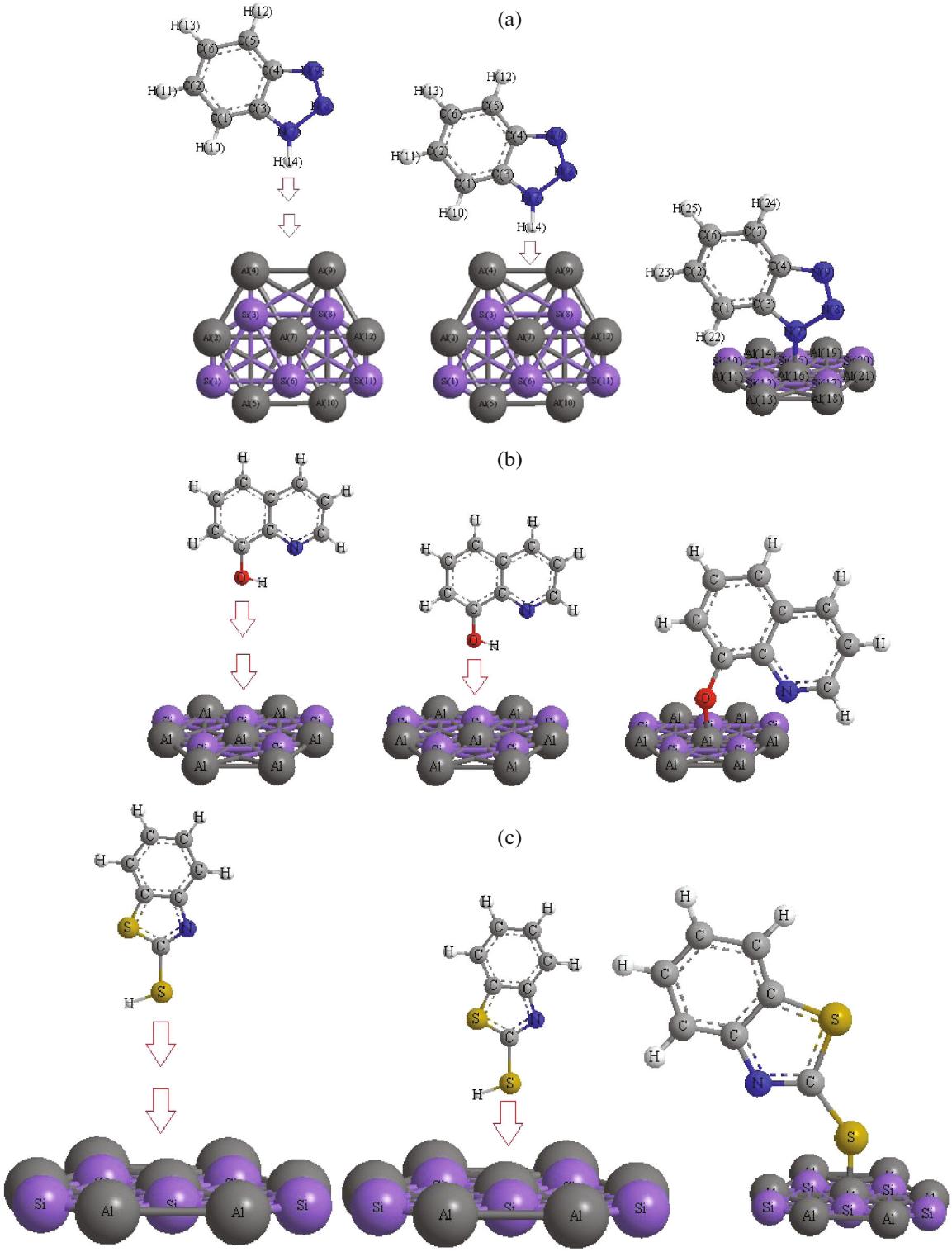

Scheme 1. Mechanism of Langmuir adsorption of the organic corrosion inhibitors of (a) benzotriazole, (b) 8-hydroxyquinoline, (c) 2-mercaptobenzothiazole onto Al(111)-alloy of Al–Si surface.

pound between the solid and liquid phases, and a monolayer attribute. The adsorbed molecules are kept on the Al(111)-alloys surface with chemisorbed inhibitors having high protection (Scheme 1).

2.3. Method of ONIOM

In this work, it has been performed the advanced ONIOM simulation. So, the combination of three levels in decreasing order of accuracy has been defined

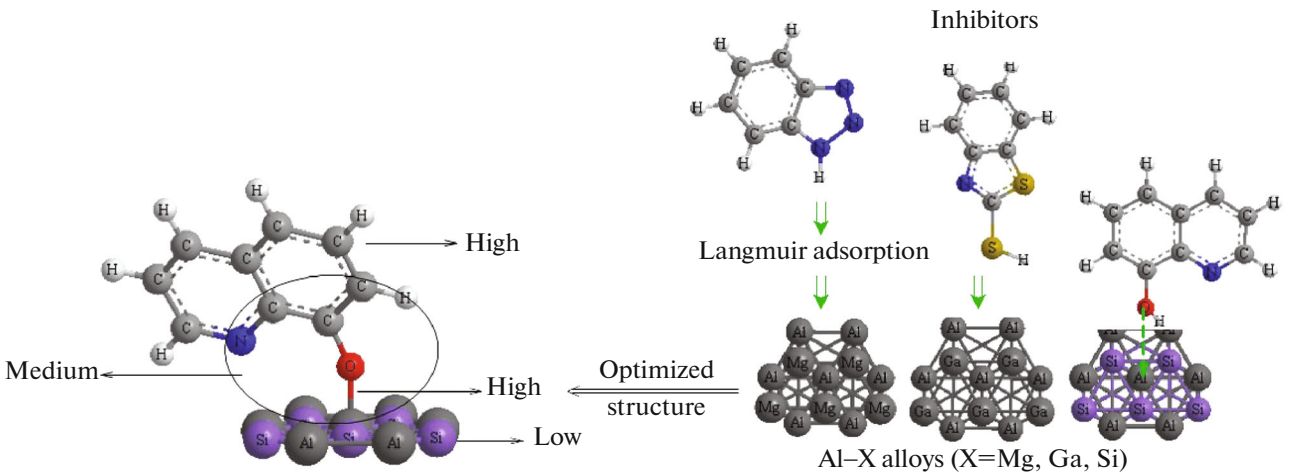

Scheme 2. The mechanism of the adsorption of benzotriazole, 8-hydroxyquinoline, 2-mercaptobenzothiazole as corrosion inhibitors onto Al(111)-alloys surface based on optimized coordination of adsorption on the Al–Mg, Al–Ga, and Al–Si surfaces.

including high, medium, and low levels of theory. High-level has been done using the DFT method of Cam-B3LYP with 6-31+G(*d*,*p*) basis set for some hydrogen, carbon, oxygen, sulfur and also some silicon atoms in the adsorption site, EPR-III basis set for nitrogen and LANL2DZ for some magnesium, aluminum and gallium atoms in the adsorption cites. Medium-level has been done on the hydrogen, carbon, nitrogen, oxygen, sulfur in the adsorption cites due to semi-empirical methods. Finally, a low-level has been performed on the other magnesium, aluminum, gallium and silicon atoms with MM2 force fields (Scheme 2) [24]

$$E_{\mathrm{ONIOM}} = E_{\mathrm{High}} + E_{\mathrm{Medium}} + E_{\mathrm{Low}}. \quad (1)$$

On the other hand, the three-layered method of ONIOM lets us to discover a larger system more exactly than the one-layered model which could behave a medium size system precisely like a ground system with acceptable accuracy [25–30].

Therefore, this three-layered pattern has been applied for effective barriers of benzotriazole, 8-hydroxyquinoline, 2-mercaptobenzothiazole adsorbed onto Al(111)-alloy surfaces containing Al–Mg, Al–Ga, and Al–Si surfaces (Scheme 2).

We have calculated the structures using the density functional theory (DFT) on the mechanisms onto Al(111)-alloy surfaces up to adsorbed in the active sites of organic inhibitors by nitrogen, oxygen and sulfur atoms of benzotriazole, 8-hydroxyquinoline, 2-mercaptobenzothiazole, respectively.

We have found that the surface binding site preferences of N-atom of benzotriazole, O-atom of 8-hydroxyquinoline, and S-atom of 2-mercaptobenzothiazole in adsorption site is largely affected by the presence of neighboring atoms. The calculated N → Al, O → Al, and S → Al pair distribution functions have indicated that the formation of clusters directs to shorter N → Al, O → Al, and S → Al bond lengths when compared to the homogeneous growth (Scheme 2).

In this article, atomic structure of the Al(111)-alloy surface has been built using GaussView 6.06.16 [31] and calculated by Gaussian 16 revision C.01 program [32] through geometry coordination. Result observations have represented that the Al(111)-alloy surface calculated with the achieved structure parameters are in good agreement with those metal-alloy attained from other experimental calculations [33–40].

Besides, heterocyclic inhibitors of benzotriazole, 8-hydroxyquinoline and 2-mercaptobenzothiazole applied in this investigation are the most tested organic compounds as corrosion inhibitors for Al and Al-alloys in both alkaline and chloride-containing solutions [41].

Furthermore, Al(111)-alloys nanosurface has been designed and compared with the structures of that Xhanari and Finsgar have represented in [42–44]. The researches have remarked that based on the applied strengthening method, commercial wrought aluminum alloys is able to categorized into two groups of non-heat treatable and heat treatable alloys made by different compositions. The non-heat treatable alloys such as Al, Al–Si, and Al–Mg have a higher corrosion resistance toward general corrosion compared to the heat treatable alloys like Al–Cu–Mg, Al–Mg–Si, Al–Zn–Mg, and etc. [45–47].

2.4. DFT Calculations

Hybrid functional is a group of approximations for the exchange-correlation energy functional in DFT (density functional theory) which combines a part of exact exchange from HF (Hartree–Fock theory)

method with the rest of the exchange-correlation energy from other information such as empirical or ab initio methodologies. Therefore, the exact exchange energy functional is illustrated by the Kohn–Sham orbitals instead of the density, so is placed as the indirect density functional. This study has applied the influence of the hybrid functional of three-parameter basis set of B3LYP (Becke, Lee, Yang, Parr) within the framework of DFT upon theoretical calculations [42–44, 48, 49].

The Al(111)-alloy consisting of Al–Mg, Al–Ga, and Al–Si surface has been built by rigid system and Z-Matrix format of which a blank line has been placed and after that the following information has been illustrated. The rigid PES has been performed at CAM-B3LYP functional [50], and employing 6-31+G(*d*,*p*)/EPRIII/LANL2DZ basis sets to assign HOMO, LUMO, Mulliken charges, nuclear magnetic resonance properties, dipole moment, thermodynamic characteristics and other quantum properties for this study [51] for benzotriazole, 8-hydroxyquinoline, 2-mercaptobenzothiazole adsorbed onto the Al(111)-alloy including Al–Mg, Al–Ga, and Al–Si surface using Gaussian 16 revision C.01 program [32]. The input files for the organic corrosion inhibitors of adsorbed onto Al–X (Mg, Ga, Si) surfaces have been provided with GaussView 6.06.16 [31]. For Al(111)-alloy surface, the small energy difference between the formations of adsorbate → Al(111)-alloy complexes can direct us to a pretty coated surface for preventing the corrosion.

3. RESULTS AND DISCUSSION

In this article, the susceptibility of organic inhibitors (benzotriazole, 8-hydroxyquinoline, and 2-mercaptobenzothiazole), characteristics of aluminum (111)-alloy surface (Al–Mg, Al–Ga, and Al–Si) and adsorption conditions are considerable.

3.1. Infrared Spectroscopy Analysis and Thermodynamic Properties

The IR spectrum for each of these compounds has been seen in the frequency range around 500–4000 cm^{-1} for benzotriazole, 8-hydroxyquinoline, and 2-mercaptobenzothiazole with the strongest peak approximately in 1600 cm^{-1}; and frequency range around 2000–10000 cm^{-1} for benzotriazole → Al–Mg, benzotriazole → Al–Ga, benzotriazole → Al–Si; 8-hydroxyquinoline → Al–Mg, 8-hydroxyquinoline → Al–Ga, 8-hydroxyquinoline → Al–Si; and 2-mercaptobenzothiazole → Al–Mg, 2-mercaptobenzothiazole → Al–Ga, 2 mercaptobenzothiazole → Al–Si with the some strongest peaks approximately between 400–1600 cm^{-1} (Fig. 1).

The infrared (IR) calculations have been accomplished for the aluminum(111)-alloys containing Al–Mg, Al–Ga, Al–Si, and three organic inhibitors including benzotriazole, 8-hydroxyquinoline, and 2-mercaptobenzothiazole adsorbed onto these alloys surface which produce the complexes of benzotriazole → Al–Mg, benzotriazole → Al–Ga, benzotriazole → Al–Si; 8-hydroxyquinoline → Al–Mg, 8-hydroxyquinoline → Al–Ga, 8-hydroxyquinoline → Al–Si; and 2-mercaptobenzothiazole → Al–Mg, 2-mercaptobenzothiazole → Al–Ga, 2-mercaptobenzothiazole → Al–Si at CAM-B3LYP level of theory employing 6-31+G(*d*,*p*)/EPRIII/LANL2DZ basis sets using Gaussian 16 revision C.01 program [32] to obtain the more accurate equilibrium geometrical parameters, physical and thermodynamic properties for each of the determined structure (Table 1).

From Table 1, it could be found that the maximum of the Langmuir adsorption isotherm plots based on ΔG°_{ads} may depend on the interactions between the inhibitor structures and the Al(111)-alloy surfaces. In fact, comparison to ΔG°_{ads} amounts confirmed a good agreement among calculated results, as well as the correctness of the selected isotherm for the adsorption process of benzotriazole → Al–Mg, benzotriazole → Al–Ga, benzotriazole → Al–Si, 8-hydroxyquinoline, 8-hydroxyquinoline → Al–Mg, 8-hydroxyquinoline → Al–Ga, 8-hydroxyquinoline → Al–Si, 2-mercaptobenzothiazole, 2-mercaptobenzothiazole → Al–Mg, 2-mercaptobenzothiazole → Al–Ga, and 2-mercaptobenzothiazole → Al–Si.

The adsorptive capacity of inhibitor structures on the Al(111)-alloys surface is approved by the ΔG°_{ads} amounts

$$\Delta G^{\circ}_{ads} = \Delta G^{\circ}_{inh\to Al-X} - (\Delta G^{\circ}_{inh} + \Delta G^{\circ}_{Al-X}); \quad X = \text{Mg, Ga, Si.} \tag{2}$$

On the basis of data in Table1, it is predicted that the adsorption of the inhibitor on the Al(111)-alloy surface might be physical and chemical nature. As shown in Table 1, all the computed ΔG°_{ads} amounts are very close, which exhibits the agreement of the evaluated data by all methods and the validity of the computations.

3.2. NMR Analysis

Then, the NMR data of isotropic (σ_{iso}), anisotropic shielding tensor (σ_{aniso}), and eigenvalues of chemical shielding including σ_{11}, σ_{22}, σ_{33} for benzotriazole → Al–Mg, benzotriazole → Al–Ga, benzotriazole → Al–Si, 8-hydroxyquinoline → Al–Mg, 8-hydroxyquinoline → Al–Ga, 8-hydroxyquinoline → Al–Si, 2-mercaptobenzothiazole → Al–Mg, 2-mercaptobenzothiazole → Al–Ga, and 2-mercaptobenzothiazole → Al–Si have been calculated using Gaussian 16 revision C.01 program [32] and reported in Tables 2–4.

The quantum chemical calculations yield the CS tensors in principal axes system to evaluate the isotro-

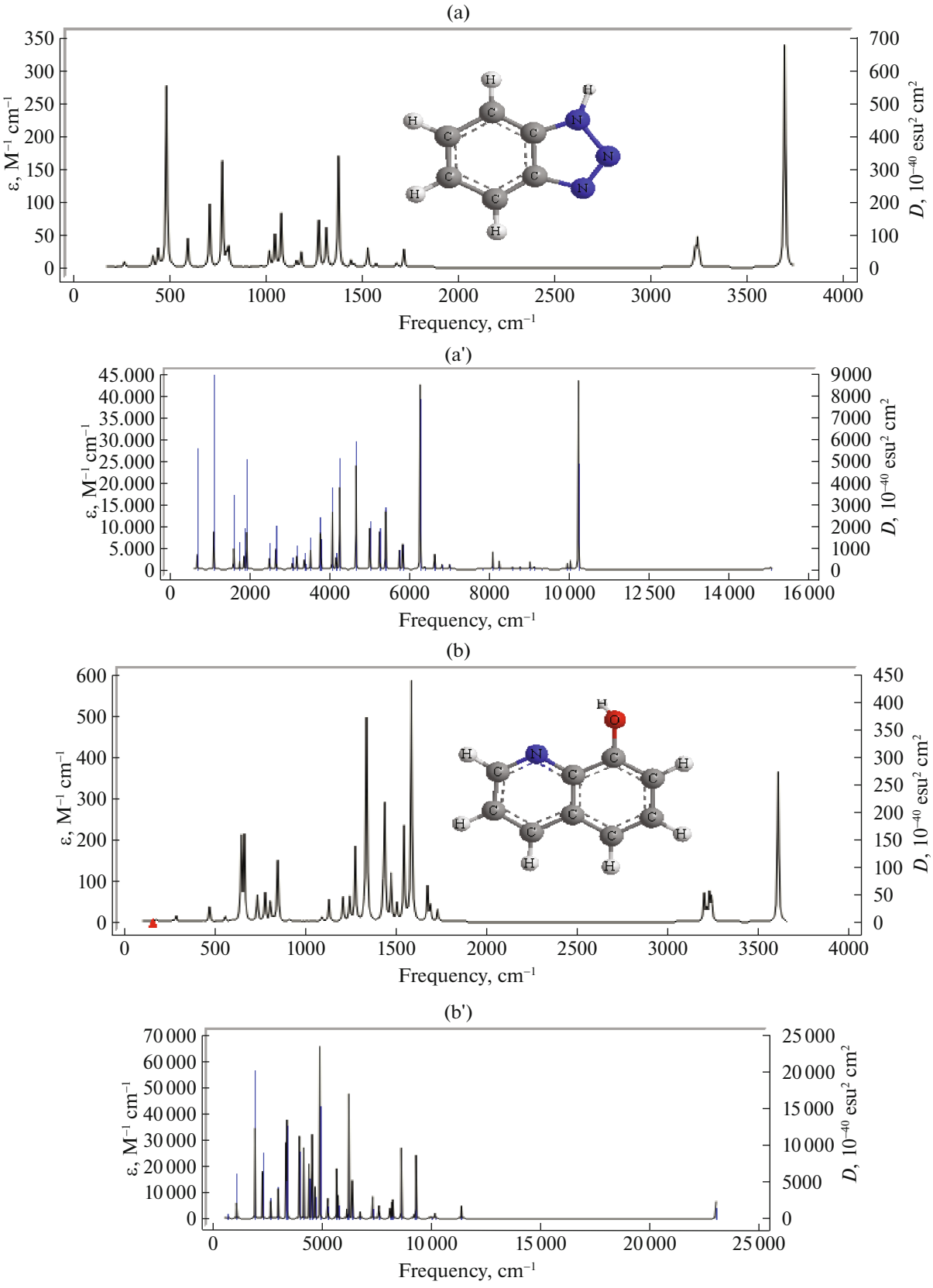

Fig. 1. Changes of IR intensity (km/mol) versus frequency (cm^{-1}) through the IR spectra for (a) benzotriazole, (a') benzotriazole → Al–Mg, (b) 8-hydroxyquinoline, (b') 8-hydroxyquinoline → Al–Ga, (c) 2-mercaptobenzothiazole, and (c') mercaptobenzothiazole → Al–Si using CAM-B3LYP method with 6-31+G(*d*,*p*)/EPRIII/LANL2DZ basis sets.

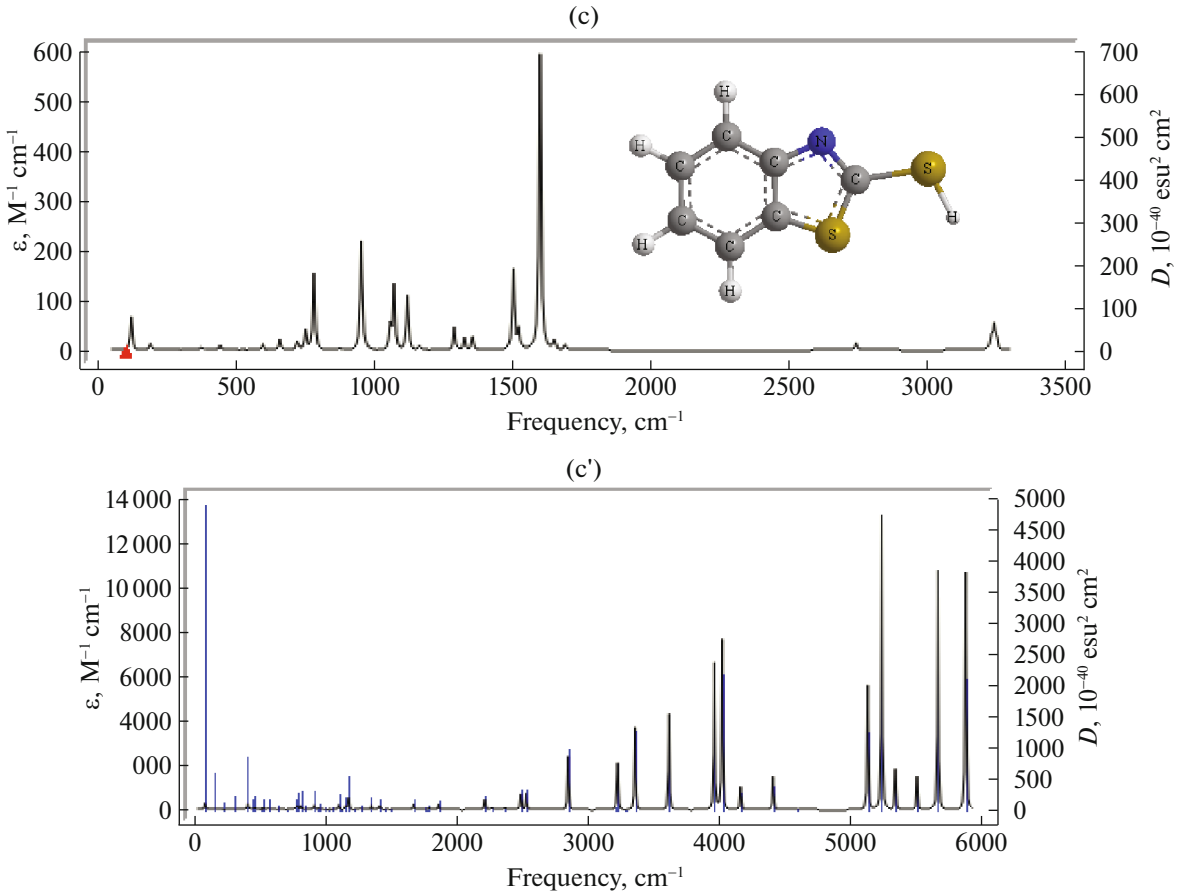

Fig. 1. (Contd.)

pic chemical-shielding (CSI) and anisotropic chemical-shielding (CSA) [52].

In fact, we have found that the isotropic and anisotropy shielding increase with the occupancy and consequently the negative charge in pyridine cycle influenced by nitrogen atom (Fig. 1). In Fig. 1, it has been exhibited that the graph of nitrogen atom has the same attitude but a considerable deviation from carbon and hydrogen atoms.

Besides, the solution of NaCl solution has influenced on the nuclear magnetic resonance data and chemical shielding of hydrogen, carbon, nitrogen, oxygen, and sulfur in benzotriazole, 8-hydroxyquinoline and 2-mercaptobenzothiazole adsorbed onto Al–Mg, Al–Ga, and Al–Si alloys. In Fig. 2, it has been indicated the chemical shielding tensors of isotropic (σ_{CSI}) and anisotropic (σ_{CSA}) of some effective atoms in the adsorption site of benzotriazole → Al–Mg, benzotriazole → Al–Ga, benzotriazole → Al–Si, 8-hydroxyquinoline → Al–Mg, 8-hydroxyquinoline → Al–Ga, 8-hydroxyquinoline → Al–Si, 2-mercaptobenzothiazole → Al–Mg, 2-mercaptobenzothiazole → Al–Ga, and 2-mercaptobenzothiazole → Al–Si (Tables 2–4). Figure 2 has certainly has focused on the aluminum shielding in the intra-atomic interaction with magnesium, gallium and silicon and simultaneously interatomic interaction with other atoms in organic inhibitors through variety of high, medium and low layers of ONIOM method.

Interatomic interactions which is related position of one, two, three, etc. atoms at a time is written as a series expansion of functional parameters with interatomic potential [53]:

$$V = \sum_{i=1}^{N} V_1(\vec{r}_i) + \sum_{i,j=1}^{N} V_2(\vec{r}_i, \vec{r}_j) + \sum_{i,j,k=1}^{N} V_3(\vec{r}_i, \vec{r}_j, \vec{r}_k) + \ldots, \quad (3)$$

where V_1 is the one-body term, V_2 the two-body term, V_3 the three body term, N the number of atoms in the system, $\vec{r}_i$ the position of atom i, $\vec{r}_j$ the position of atom j, $\vec{r}_k$ the position of atom k and i, j, k are indices that sprain around atom positions.

Intra-atomic interactions consist of Al(7)–Mg, Al(7)–Ga, Al(7)–Si and interatomic interaction are N(7) → Al(16)–Mg, N(7) → Al(16)–Ga, N(7) → Al(16)–Si; O(11) → Al(18)–Mg, O (11) → Al(18)–

Table 1. The physico-chemical properties of adsorption for benzotriazole, 8-hydroxyquinoline, 2-mercaptobenzothiazole as corrosion inhibitors on the aluminum alloys surface including Al–Al, Al–Mg, Al–Ga, and Al–Si in NaCl solution at 300 K

Compound	$\Delta E^\circ \times 10^{-4}$, kcal/mol	$\Delta H^\circ \times 10^{-4}$, kcal/mol	$\Delta G^\circ \times 10^{-4}$, kcal/mol	$\Delta G^\circ_{ads} \times 10^{-4}$, kcal/mol	S°, cal/(K mol)	Dipole moment, D
Al–Al	−179.9207	−179.9206	−179.9229	—	76.078	2.0432
Al–Mg	−166.2904	−166.2904	−166.2926	—	75.228	0.3215
Al–Ga	−701.4839	−701.4838	−701.4861	—	77.743	8.7320
Al–Si	−193.9035	−193.9035	−193.9057	—	75.709	0.9580
Benzotriazole	−24.5172	−24.5172	−24.5196	—	80.255	3.3166
Benzotriazole → Al–Al	−204.3672	−204.3672	−204.3699	0.0726	89.924	5.5621
Benzotriazole → Al–Mg	−190.7951	−190.7950	−190.7977	0.0145	88.808	3.9183
Benzotriazole → Al–Ga	−725.9452	−725.9451	−725.9478	0.0579	90.854	6.6691
Benzotriazole → Al–Si	−218.2713	−218.2752	−218.2793	0.1460	137.5839	5.6456
8-Hydroxyquinoline	−29.5527	−29.5526	−29.5551	—	83.336	1.6389
8-Hydroxyquinoline → Al–Al	−209.4315	−209.4314	−209.4345	0.0435	103.854	4.1199
8-Hydroxyquinoline → Al–Mg	−195.8071	−195.8071	−195.8099	0.0378	94.571	6.0496
8-Hydroxyquinoline → Al–Ga	−730.9885	−730.9885	−730.9915	0.0497	101.042	8.4636
8-Hydroxyquinoline → Al–Si	−223.3408	−223.3407	−223.3438	0.1170	102.930	3.0399
2-Mercaptobenzothiazole	−69.5235	−69.5234	−69.5260	—	85.643	2.5108
2-Mercaptobenzothiazole→ Al–Al	−249.3654	−249.3653	−249.3682	0.0807	96.277	0.3513
2-Mercaptobenzothiazole → Al–Mg	−235.7773	−235.7773	−235.7800	0.0386	90.329	5.2949
2-Mercaptobenzothiazole → Al–Ga	−770.9160	−770.9160	−770.9188	0.0933	94.313	10.4893
2-Mercaptobenzothiazole → Al–Si	−263.2566	−263.2565	−263.2594	0.1723	96.640	2.8880

Ga, O(11) → Al(18)–Si; S(10) → Al(17)–Mg, S(10) → Al(17)–Ga, S(10) → Al(17)–Si based on the of CAM-B3LYP/6-31+G(*d*,*p*)/EPR-III/LANL2DZ quantum mechanics calculations using Gaussian 16 revision C.01 program [32] (Fig. 2).

Form Fig. 2, it has been observed that Al–Si with highest fluctuation in the shielding tensors of NMR spectrum generated by intra-atomic interaction directs us to the most influence in the neighbor atoms generated by interatomic reaction.

3.3. Charge Density Analysis

Through observing the intra/inter interactions between organic inhibitor of benzotriazole, 8-hydroxyquinoline, and 2-mercaptobenzothiazole with the Al(111)-alloy surface of Al–Mg, Al–Ga, and Al–Si, and consequently formation of adsorbed surfaces of benzotriazole → Al–Mg, benzotriazole → Al–Ga, benzotriazole → Al–Si, 8-hydroxyquinoline → Al–Mg, 8-hydroxyquinoline → Al–Ga, 8-hydroxyquinoline → Al–Si, 2-mercaptobenzothiazole → Al–Mg, 2-mercaptobenzothiazole → Al–Ga, and 2-mercaptobenzothiazole → Al–Si (Tables 2–4) based on Langmuir adsorption using CAM-B3LYP/6-31+G(*d*, *p*)/EPR-III/LANL2DZ level of theory, CDD (the charge density difference) for these structures at the adsorption site has been estimated and plotted in Fig. 3 with the following equation:

$$\Delta Q_{ads} = Q_{inhibitor\rightarrow(Al-X)surface} - (Q_{inhibitor} + Q_{(Al-X)surface}), \quad (4)$$

where $Q_{inhibitor\rightarrow(Al-X)surface}$ is the charge density of the adsorption system; $Q_{inhibitor}$ and $Q_{(Al-X)surface}$ are the charge densities of non-interacting of organic inhibitor and that of the Al(111)-alloy surface.

Based on Fig. 3, the electronic charge for aluminum atom through intra-atomic interaction with gallium and silicon atoms in alloys surface containing Al–Mg, Al–Ga, and Al–Si and also through interatomic interaction with organic heterocyclic inhibitors of benzotriazole, 8-hydroxyquinoline, 2-mercaptobenzothiazole has been plotted. The adsorption site due to interatomic interaction in the fragments of the active sites for benzotriazole → Al–X, 8-hydroxyquinoline → Al–X, 2-mercaptobenzothiazole → Al–X (X = Mg, Ga, Si) are N → Al, O → Al, S → Al, respectively. The elements of N, O, and S with high electronegativity and non-bonded pair electrons have the principal role for transferring the electronic charge to the nanosurface of Al(111)-alloys. Benzotriazole → Al–Si, 8-hydroxyquinoline → Al–Si, 2-mercaptobenzothiazole → Al–Si have shown more fluctuation than inhibitors → Mg/Ga. Therefore, it has been rep-

Table 2. NMR properties of some atoms of benzotriazole in ppm adsorbed onto Al–Mg, Al–Ga, and Al–Si alloys

Atom number	σ_{11}	σ_{22}	σ_{33}	σ_{CSI}	σ_{CSA}	Q
Benzotriazole → Al–Mg						
C3	−1125.5123	372.8979	531.1039	−73.8368	907.4111	−7.2779
C4	−5220.1079	100.4783	1472.1446	−1215.8283	4031.9594	2.0281
N7	−7502.2450	360.0701	864.0878	−2092.6957	4435.1753	−19.9952
N8	−1597.2258	54.7614	1740.8142	66.1166	2512.0464	−7.7458
N9	−3704.2994	243.7586	2221.2132	−413.1092	3951.4836	1.4381
Mg11	−49.4619	36.3814	79.9896	22.3030	86.5299	3.1248
Mg15	−108.5967	30.3689	94.7758	5.5160	133.8897	3.5268
Al16	−112.7434	38.1329	124.0921	16.4939	161.3973	5.0965
Mg17	−90.6992	45.5780	93.9477	16.2755	116.5082	4.222
Benzotriazole → Al–Ga						
C3	22.3798	218.6147	425.1691	222.0545	304.6718	−19.4454
C4	−343.5095	144.7520	251.7808	17.6744	351.1595	−9.0856
N7	379.3393	446.6173	548.8068	458.2545	135.8285	−21.0487
N8	339.7936	404.9057	513.0378	419.2457	140.6881	−21.3932
N9	−1720.0544	50.7708	292.4971	−458.9288	1127.1389	−12.8061
Ga12	42.8274	47.2357	92.9890	61.0173	47.9574	22.9988
Ga15	23.6390	51.5058	76.2863	50.4770	38.7139	22.9985
Al16	31.9241	55.7063	77.8606	55.1637	34.0454	5.0031
Ga17	25.7035	36.6767	81.6323	48.0042	50.4422	23.0009
Benzotriazole → Al–Si						
C3	−14.5666	103.0843	190.0033	92.8403	145.7444	0.4725
C4	3.2091	60.8189	95.5729	53.2003	63.5588	0.4550
N7	−783.7598	−294.1715	384.2896	−231.2139	923.2552	−3.21033
N8	−913.6225	−532.9451	284.8140	−387.2512	1008.0978	0.4314
N9	−1065.1543	−110.4888	188.9914	−328.8839	776.8130	−0.1498
Si12	−332.3086	529.3786	609.5611	268.8770	511.0261	−19.407
Si14	56.6034	572.5635	731.5313	453.5661	416.9479	−33.1297
Al16	−87.0189	−7.7344	78.3778	−5.4585	125.7545	16.6867
Si17	−179.8395	179.4616	644.6333	214.7518	644.8222	−14.1193

resented the detailed characteristics of inter and intra interaction of inhibitors → Al–X (X = Mg, Ga, Si) alloys nanosurface through potential energy.

3.4. Potential Energy of Interatomic Interaction

The interatomic potential explains the interaction between a pair of atoms or the interaction of an atom with a group of atoms in a condensed phase. When binding happens, we can observe the potential having both an attractive and a repulsive component [54–56].

The figure of the potential energy as a function of lattice distance with the interval of interatomic interaction in a solid is described that an atom in the ideal crystalline solid feels the same potential through the other atoms in the material. Accompanying Eq. (8), it has been investigated the Morse potential which is applied for molecular vibrations and solids [57] and also excited the functional form of more accurate potentials like the bond-order potentials:

$$V_{\mathrm{M}}(r) = D_e\left(e^{-2\alpha(r-r_e)} - 2e^{-\alpha(r-r_e)}\right), \quad (5)$$

where D_e is the equilibrium bond energy and r_e the bond distance. Therefore, the optimized potential energy of interatomic interaction for benzotriazole → Al–Mg, benzotriazole → Al–Ga, benzotriazole → Al–Si; 8-hydroxyquinoline → Al–Mg, 8-hydroxyquinoline → Al–Ga, 8-hydroxyquinoline → Al–Si; and 2-mercaptobenzothiazole → Al–Mg, 2-mercaptobenzothiazole → Al–Ga, 2-mercaptobenzothiazole → Al–Si have been measured (Table 5). Then, the distance between nitrogen atom in benzotriazole, sulfur

Table 3. NMR properties of some atoms of 8-hydroxyquinoline in ppm adsorbed onto Al–Mg, Al–Ga, and Al–Si alloys

Atom number	σ_{11}	σ_{22}	σ_{33}	σ_{CSI}	σ_{CSA}	Q
8-Hydroxyquinoline → Al–Mg						
C1	−1392.2174	−185.2194	997.9485	−193.1628	1786.6669	−6.7733
C3	−327.1419	−24.5372	219.8056	−43.9578	395.6452	−2.6363
N7	189.7427	660.7033	2128.3299	992.9253	1703.1069	−11.9009
O11	489.0241	597.2717	919.4824	668.5928	376.3345	−19.9897
Mg13	67.8344	77.3476	104.8642	83.3488	32.2732	2.0531
Mg17	37.2749	60.5575	104.6769	67.5031	55.7607	4.1278
Al18	49.5021	76.4509	147.2902	91.0811	91.0811	5.1597
Mg19	39.1296	54.1029	96.6752	63.3026	50.0590	4.0866
8-Hydroxyquinoline → Al–Ga						
C1	58.5543	215.5265	357.7643	210.6150	220.7239	−17.2651
C2	−88.3609	122.4737	155.0504	63.0544	137.9940	−13.2503
C3	147.3772	245.0521	295.0045	229.1446	98.7898	−9.7397
O11	412.3112	545.6906	622.1284	526.7101	143.1275	−20.0680
Ga14	22.3493	27.5308	92.1722	47.3508	67.2322	23.0064
Ga17	8.9870	30.1500	64.8316	34.6562	45.2631	22.9966
Al18	23.7628	27.3007	86.2681	45.7772	60.7364	4.9780
Ga19	17.6923	42.0036	78.6459	46.1139	48.7979	22.9944
H24	2.9408	36.0016	57.9174	32.2866	38.4462	−3.0197
8-Hydroxyquinoline → Al–Si						
C1	−119.0343	87.8036	462.4873	143.7522	478.1027	0.7248
C2	−263.4597	−9.8199	165.6544	−35.8751	302.2942	−0.0414
C3	−66.9617	98.2121	431.9174	154.3892	416.2922	0.6769
O11	−692.2351	−4.5925	385.3007	−103.8423	733.7144	−0.5657
Si14	351.9919	407.3696	1115.9205	625.0940	736.2397	−31.7887
Si17	−3439.0415	441.8579	1311.5255	−561.8860	2810.1173	−33.4693
Al18	−158.2447	57.4176	105.4744	1.5491	155.8880	23.6131
Si19	−96.0303	308.9690	1248.9763	487.3050	1142.5070	−32.8389
H24	−64.4227	36.2199	59.1951	10.3307	73.2965	0.2705

atom in 2-mercaptobenzothiazole, and oxygen atom in 8-hydroxyquinoline, respectively, with Al–Mg, Al–Ga, and Al–Si nanosurface has been evaluated (Table 5). Finally, the changes of potential energy for these complexes and interatomic integration distance has been plotted in Fig. 4 with ($R^2 = 0.9742$).

Based on Fig. 4, it can be assumed that for benzotriazole → Al–Mg, benzotriazole → Al–Ga, benzotriazole → Al–Si; 8-hydroxyquinoline → Al–Mg, 8-hydroxyquinoline → Al–Ga, 8-hydroxyquinoline → Al–Si; and 2-mercaptobenzothiazole → Al–Mg, 2-mercaptobenzothiazole → Al–Ga, 2-mercaptobenzothiazole → Al–Si, Lennard-Jones potential as an intermolecular pair potential can be described [58]:

$$V_{LJ}(r) = 4\varepsilon\left[\left(\frac{\sigma}{r}\right)^{12} - \left(\frac{\sigma}{r}\right)^{6}\right], \quad (6)$$

where ε is the depth of the potential well, and σ is the interval at which the potential = 0. The attractive term proportional to $1/r^6$ in the potential comes from the balancing the van der Waals forces, while the $1/r^{12}$ repulsive term is much more approximate [59].

El-Shafei and his coworkers have reported that the inhibitive action was dependent on the number of active centers in the corrosion inhibitor molecule, molecular size, and the mode of adsorption [60]. The results of Table 5 has approved that the existence of two active centers of sulfur in 2-mercaptobenzothiazole, high molecular size of this compound, application of the non-heat treatable surface of Al–Al (pure), Al–Si, and Al–Mg (alloys) cause high corrosive inhibition for 2-mercaptobenzothiazole → Al–Ga > Al–Al > Al–Mg ≈ Al–Si. After that, the presence of O atom in 8-hydroxyquinoline and N atom in ben-

Table 4. NMR properties of some atoms of 2-mercaptobenzothiazole in ppm adsorbed onto Al–Mg, Al–Ga, and Al–Si alloys

Atom number	σ_{11}	σ_{22}	σ_{33}	σ_{CSI}	σ_{CSA}	Q
2-Mercaptobenzothiazole → Al–Mg						
S7	297.0754	977.2751	1363.9304	879.4270	726.7552	−19.3193
C8	221.7712	276.7313	586.6597	361.7207	337.4084	−13.0365
N9	238.5684	345.3316	382.1882	322.0294	90.2381	1.6243
S10	484.4073	972.2207	1092.3442	849.6574	364.0302	−19.9362
Mg12	62.8835	69.9114	126.3563	86.3837	59.9589	4.0734
Mg16	62.4954	70.8614	126.9126	86.7565	60.2341	4.0805
Al17	65.2688	95.6722	171.6135	110.8515	91.1430	4.9773
Mg18	46.2320	92.1122	116.9185	85.0876	47.7464	2.6135
2-Mercaptobenzothiazole → Al–Ga						
S7	299.1033	364.6196	863.2117	508.9782	531.3503	−20.4061
C8	184.5202	367.1342	531.1608	360.9384	255.3336	−22.3068
N9	136.6296	337.3127	430.7796	301.5740	193.8085	−15.2608
S10	393.1748	830.4731	985.9082	736.5187	374.0842	−19.9998
Ga13	35.2826	77.6400	95.9985	69.6404	39.5373	23.0031
Ga16	3.4714	42.6913	135.4960	60.5529	112.4147	22.9997
Al17	20.5777	63.1659	117.6587	67.1341	75.7869	5.0008
Ga18	−1.5304	42.3704	105.7307	48.8569	85.3107	22.9993
2-Mercaptobenzothiazole → Al–Si						
S7	77.9670	326.3346	402.6839	268.9952	200.5330	0.4274
C8	−78.2160	39.7359	103.8114	21.7771	123.0515	0.1845
N9	−491.3549	131.6031	589.9647	76.7377	769.8406	−0.1668
S10	−961.4697	−179.9695	1342.9182	67.1596	1913.6378	−0.5745
Si13	−347.9644	336.8615	715.0257	234.6409	720.5772	−30.7040
Si16	−596.7718	446.0832	785.3435	211.5516	860.6878	−32.8600
Al17	3.4816	44.2372	88.4281	45.3823	64.5687	17.1290
Si18	104.2951	262.8661	620.5093	329.2235	436.9287	−31.8092

Table 5. Potential energy (kcal/mol) of interatomic interaction and distance (Å) of nitrogen atom in benzotriazole, sulfur atom in 2-mercaptobenzothiazole, and oxygen atom in 8-hydroxyquinoline, respectively, with Al–Mg, Al–Ga, and Al–Si nanosurface

Inhibitor	Potential energy × 10^{-4}, kcal/mol	Distance	(Å)
Benzotriazole → Al–Al	−204.3672	N(7) → Al(16)	1.9300
Benzotriazole → Al–Mg	−190.7951	N(7) → Al(16)	1.9152
Benzotriazole → Al–Ga	−725.9452	N(7) → Al(16)	1.9714
Benzotriazole → Al–Si	−170.8027	N(7) → Al(16)	1.9400
8-Hydroxyquinoline → Al–Al	−209.4315	O(11) → Al(18)	1.9099
8-Hydroxyquinoline →Al–Mg	−195.8071	O(11) → Al(18)	1.9098
8-Hydroxyquinoline →Al–Ga	−730.9885	O(11) → Al(18)	1.9100
8-Hydroxyquinoline → Al–Si	−223.3408	O(11) → Al(18)	1.9101
2-Mercaptobenzothiazole → Al–Al	−249.3654	S(10) → Al(17)	2.2001
2-Mercaptobenzothiazole → Al–Mg	−235.7773	S(10) → Al(17)	2.1999
2-Mercaptobenzothiazole → Al–Ga	−770.9160	S(10) → Al(17)	2.2001
2-Mercaptobenzothiazole → Al–Si	−263.2566	S(10) → Al(17)	2.2000

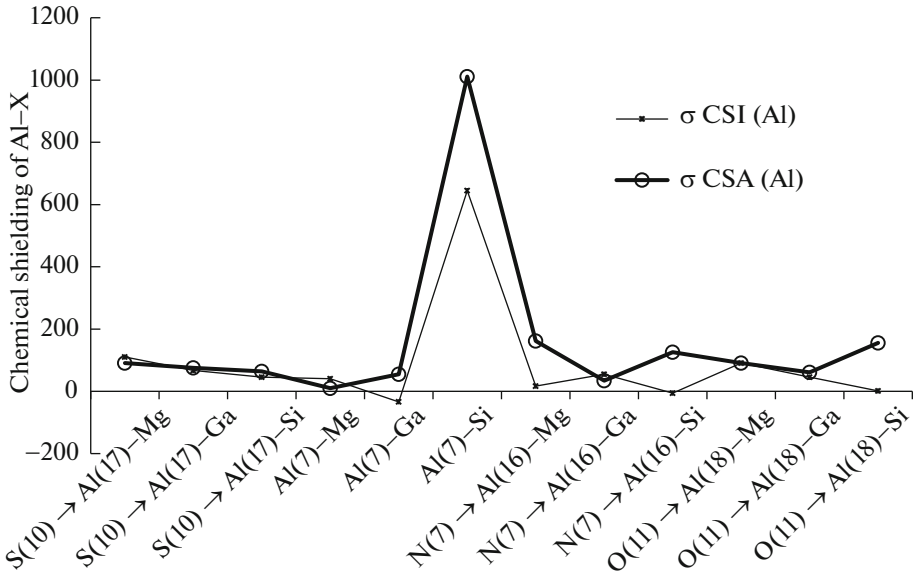

Fig. 2. The NMR plot of isotropic (σ_{iso}) and anisotropic (σ_{aniso}) shielding tensors for aluminum atom through intra-atomic interaction with gallium and silicon in alloys surface [Al–X (X = Mg, Ga, Si)] and through interatomic interaction with organic inhibitors in the adsorption site (N → Al, O → Al, S → Al) of calculated by level of theory CAM-B3LYP/6-31+G(*d*,*p*)/EPR-III/LANL2DZ.

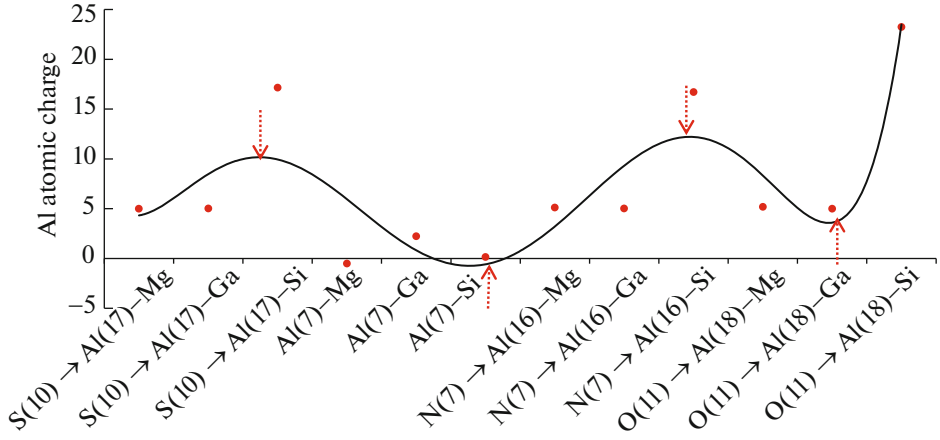

Fig. 3. Calculated electronic charge for Al through intra-atomic interaction with Ga and Si in alloys surface [Al–X (X = Mg, Ga, Si)] and through interatomic interaction with organic inhibitors in the adsorption site (N → Al, O → Al, S → Al) of calculated by level of theory CAM-B3LYP/6-31+G(*d*,*p*)/EPR-III/LANL2DZ.

zotriazole, respectively, exhibits the ability of these compounds for preventing corrosion through Langmuir adsorption mechanism as 8-hydroxyquinoline → Al–Ga > Al–Al > Al–Mg ≈ Al–Si and then benzotriazole → Al–Ga > Al–Al > Al–Mg ≈ Al–Si, respectively.

3.5. HOMO, LUMO and UV–Vis Analysis

The ionization causes the highest occupied molecular orbital (HOMO) energy and the electron affinity produces the lowest unoccupied molecular orbital (LUMO) energy which have been calculated and reported for benzotriazole, 8-hydroxyquinoline and 2-mercaptobenzothiazole in Scheme 3. The HOMO (a.u.), LUMO (a.u.), and band energy gap ($\Delta E = E_{LUMO} - E_{HOMO}$) (eV) presented the pictorial explanation of the frontier molecular orbital's and their respective positive and negative zones which are an important factor for identifying the molecular characteristics of effective compounds in these organic inhibitors (Scheme 3).

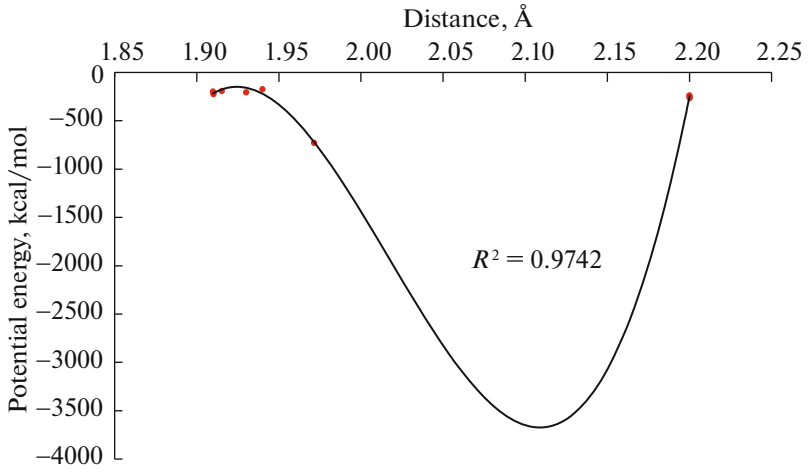

Fig. 4. The graph of potential energy (kcal/mol) of interatomic interaction versus distance (Å) of nitrogen atom in benzotriazole, sulfur atom in 2-mercaptobenzothiazole, and oxygen atom in 8-hydroxyquinoline, with aluminum atom in Al–Mg, Al–Ga, and Al–Si nanosurface, respectively.

On the other hand, the HOMO shows the capability for giving an electron while the LUMO as an electron acceptor exhibits the capability for achieving an electron. Therefore, the energy gap ($\Delta E = E_{LUMO} - E_{HOMO}$) indicates the energy difference between frontier HOMO and LUMO orbital introducing the stability for the structure and unravels the chemical activity of the molecule. In this work, energy gap establishes how benzotriazole, 8-hydroxyquinoline, and 2-mercaptobenzothiazole adsorb on the Al(111)-alloy surface at B3LYP/6-311+G(*d*,*p*)/EPR-III/LANL2DZ quantum method. Besides, frontier molecular orbitals run an important function in the optical and electrical properties like in UV–Vis spectra [61].

The energy gap between HOMO and LUMO has distinguished the attributes of molecular electrical transport [62]. Through Frank–Condon principle; the maximum absorption peak (max) depends on an UV–Vis spectrum to vertical excitation.

In this verdict, TD-DFT/6-31+G(*d*,*p*)/EPR-III/LANL2DZ computations have been done to identify the low-lying excited states of benzotriazole, 8-hydroxyquinoline and 2-mercaptobenzothiazole adsorbed on the Al(111)-alloy surface. The results consist of the vertical excitation energies, oscillator strength and wavelength which have been introduced in Figs. 5a–5c.

In fact, based on the computed amounts of UV–Vis spectra for benzotriazole, 8-hydroxyquinoline and 2-mercaptobenzothiazole adsorb on the Al(111)-alloy surface, there are maximum adsorption bands between 200–280 nm for benzotriazole, 225–350 nm for 8-hydroxyquinoline, and 210–280 nm for 2-mercaptobenzothiazole, respectively (Figs. 5a–5c); and maximum adsorption bands for benzotriazole, 8-hydroxyquinoline, and 2-mercaptobenzothiazole has observed around 230, 300, and 240 nm, respectively (Figs. 5a–5c).

4. CONCLUSIONS

In this research, the adsorption and diffusion of benzotriazole, 8-hydroxyquinoline, and 2-mercaptobenzothiazole on the Al(111)-alloy surface have been investigated based on Langmuir theory using ONIOM method with high, medium and low levels of EPR-III/6-31+G(*d*,*p*)/LANL2DZ, semi-empirical and MM2 basis sets, respectively by Gaussian 16 revision C.01 program.

In this work, the efficiency of the organic inhibitors as the aluminum(111)-alloy coating has been studied through the electronic, thermodynamic features and characteristics of the environmental condition which results the complexes of benzotriazole → Al–Mg, benzotriazole → Al–Ga, benzotriazole → Al–Si; 8-hydroxyquinoline → Al–Mg, 8-hydroxyquinoline → Al–Ga, 8-hydroxyquinoline → Al–Si; and 2-mercaptobenzothiazole → Al–Mg, 2-mercaptobenzothiazole → Al–Ga, 2-mercaptobenzothiazole → Al–Si.

An elaborate investigation for the mechanism of local minima in the adsorption potential energy landscape represents that the intact benzotriazole, 8-hydroxyquinoline and 2-mercaptobenzothiazole adsorb with the aromatic ring parallel to the Al(111)-alloys surface. In fact, it has been observed that the inhibition effectiveness of these compounds has increased with enhancement of purity and molecular weight. Therefore, the results have approved that the inhibition efficiency is ordered as: Al–Ga > Al–Al >

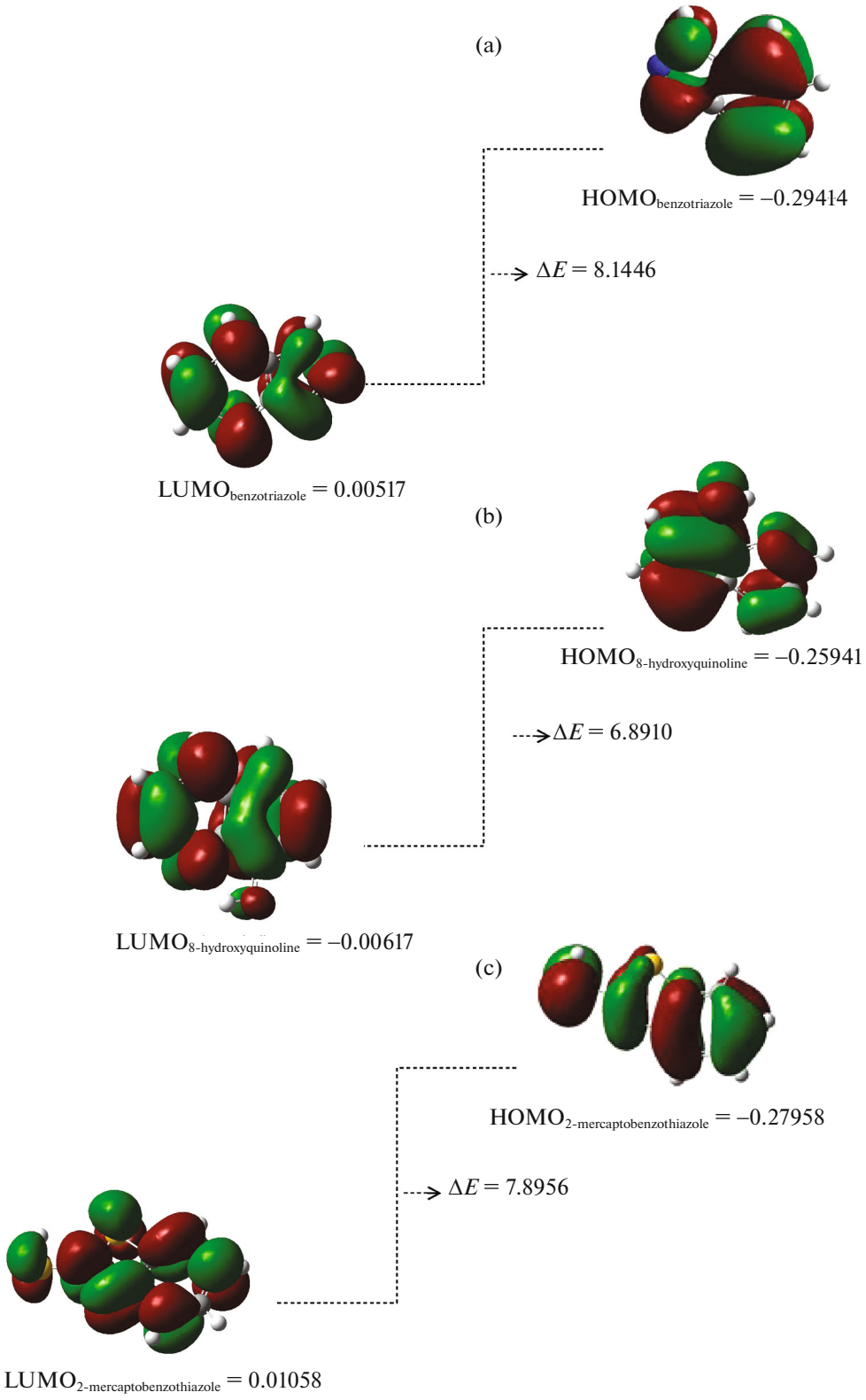

Scheme 3. The HOMO, LUMO and band energy gap (eV) for three organic inhibitors for (a) benzotriazole, (b) 8-hydroxyquinoline, and (c) 2-mercaptobenzothiazole.

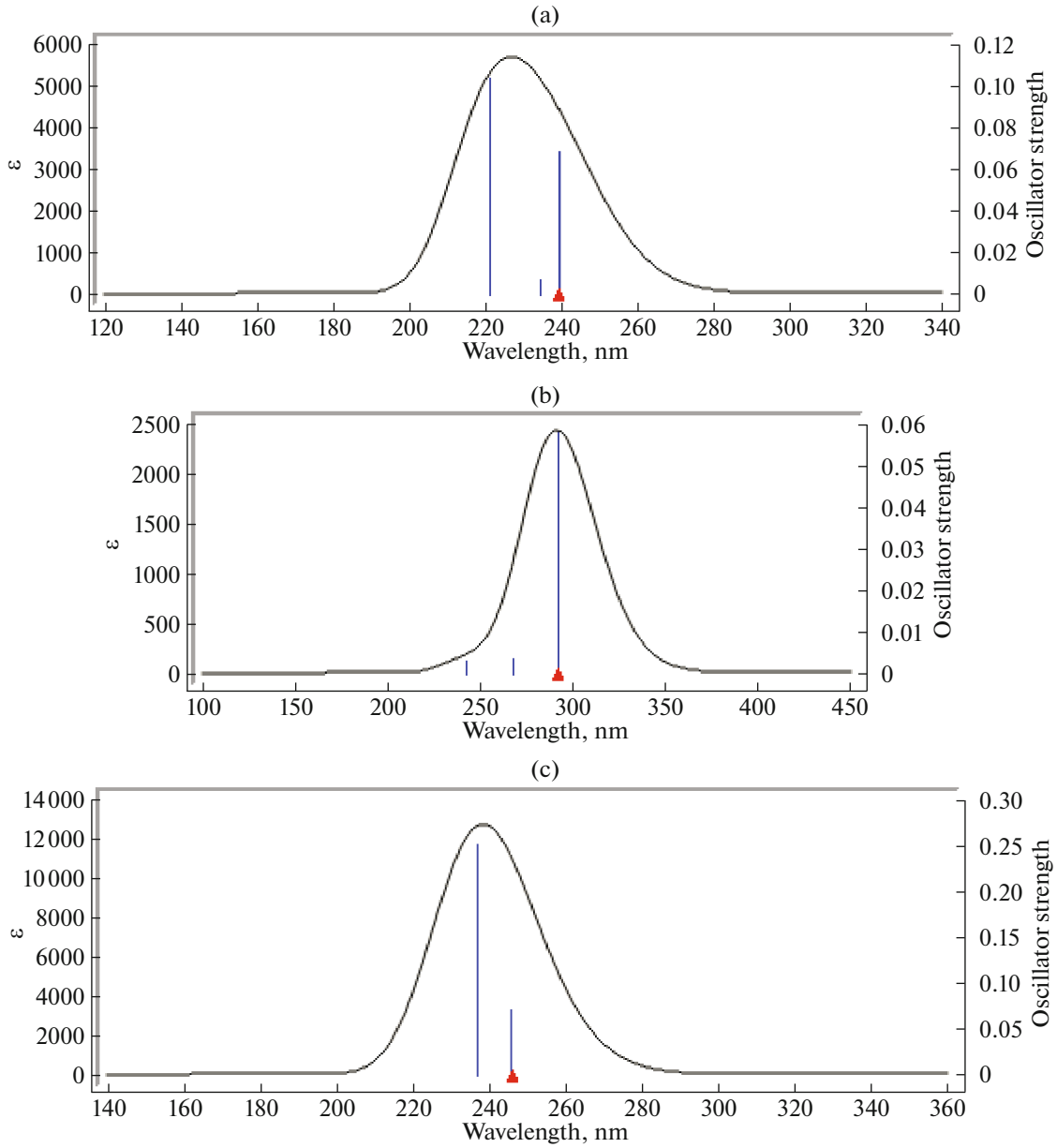

Fig. 5. UV–Vis spectroscopy of (a) benzotriazole, (b) 8-hydroxyquinoline, and (c) 2-mercaptobenzothiazole adsorbed on the Al(111)-alloy surface.

Al–Mg ≈ Al–Si. The adsorbed compound molecules of benzotriazole, 8-hydroxyquinoline, 2-mercaptobenzothiazole and their complexes [adsorbate → Al–X (X = Mg/Ga/Si)] showed a blocking effect on the Al–X (X = Mg/Ga/Si) nanosurface against the corrosion. In addition, 2-mercaptobenzothiazole can produce a stable interatomic interaction of S → Al in the Al–Ga, Al–Al, Al–Mg, Al–Si, respectively, higher than 8-hydroxyquinoline with interatomic interaction of O → Al and benzotriazole with interatomic interaction of N → Al. It has to be pointed out that the authors used considerably pure and mixed of aluminum surface for corrosion inhibition study.

CONFLICT OF INTEREST

The authors declare that they have no conflicts of interest.

REFERENCES

1. F. Lasagni, A. Lasagni, E. Marks, C. Holzapfel, F. Mücklich, and H. Degischer, Acta Mater. **55**, 3875 (2007).
2. F. Mollaamin and M. Monajjemi, J. Biol. Tribol. Corros. **9**, 33 (2023). https://doi.org/10.1007/s40735-023-00751-y
3. Z. Asghar, G. Requena, and F. Kubel, Mater. Sci. Eng. A **527**, 5691 (2010).

4. F. Stadler, H. Antrekowitsch, W. Fragner, H. Kaufmann, and P. Uggowitzer, Int. J. Cast Met. Res. **25**, 215 (2012).
5. Y. Boughoues, M. Benamira, L. Messaadia, and N. Ribouh, Colloids Surf., A **593**, 124610 (2020). https://doi.org/10.1016/j.colsurfa.2020.124610
6. M. Özcan, R. Solmaz, G. Kardaš, and İ. Dehri, Colloids Surf., A **325**, 57 (2008). https://doi.org/10.1016/j.colsurfa.2008.04.031
7. J. Saranya, M. Sowmiya, P. Sounthari, K. Parameswari, S. Chitra, and K. Senthilkumar, J. Mol. Liq. **216**, 42 (2016). https://doi.org/10.1016/j.molliq.2015.12.096
8. T. A. S. Guimarães et al., J. Mater. Res. Technol. **9**, 7104 (2020). https://doi.org/10.1016/j.jmrt.2020.05.019
9. M. Ozcan, Acta Phys.-Chim. Sin. **24**, 1387 (2008). https://doi.org/10.1016/S1872-1508(08)60059-5
10. M. Mobin and R. Aslam, Process. Saf. Environ. Prot. **114**, 279 (2018). https://doi.org/10.1016/j.psep.2018.01.001
11. A. Singh et al., Molecules **20**, 15122 (2015). https://doi.org/10.3390/molecules200815122
12. S. A. Ali, M. A. J. Mazumder, M. K. Nazal, and H. A. Al-Muallem, Arab. J. Chem. **13**, 242 (2020). https://doi.org/10.1016/j.arabjc.2017.04.005
13. H. Amar, J. Benzakour, A. Derja, D. Villemin, and B. Moreau, J. Electroanal. Chem. **558**, 131 (2003). https://doi.org/10.1016/S0022-0728(03)00388-7
14. M. S. El-Sayed, Int. J. Electrochem. Sci. **6**, 1479 (2011).
15. E. S. Sherif, Molecules **19**, 9962 (2014). https://doi.org/10.3390/molecules19079962
16. D. Yang, M. Zhang, J. Zheng, and H. Castaneda, RSC Adv. **5**, 95160–95170 (2015). https://doi.org/10.1039/C5RA14556B
17. G. Amberchan et al., ACS Appl. Nano Mater. **5** (2), 2636–2643 (2022). https://doi.org/10.1021/acsanm.1c04331
18. M. Finšgar and I. Milošev, Corros. Sci. **52**, 2737 (2010). https://doi.org/10.1016/j.corsci.2010.05.002
19. A. Y. Shen, S. N. Wu, and C. T. Chiu, J. Pharm. Pharmacol. **51**, 543 (1999). https://doi.org/10.1211/0022357991772826
20. P. A. J. Cabassi et al., J. South Afr. Inst. Mining Metall. **83** (11), 270 (1983).
21. K. Xhanari and M. Finsğar, RSC Adv. **6**, 62833 (2016).
22. M. E. Mashuga, L. O. Olasunkanmi, and E. E. Ebenso, J. Mol. Struct. **1136**, 127 (2017). https://doi.org/10.1016/j.molstruc.2017.02.002
23. M. Monajjemi, L. Mahdavian, F. Mollaamin, and M. Khaleghian, Russ. J. Inorg. Chem. **54**, 1465 (2009). https://doi.org/10.1134/S0036023609090216
24. M. Svensson, S. Humbel, R. D. J. Froese, T. Matsubara, S. Sieber, and K. Morokuma, J. Phys. Chem. **100**, 19357 (1996). https://doi.org/10.1021/jp962071j
25. L. Mahdavian and M. Monajjemi, Microelectron. J. **41**, 142 (2010). https://doi.org/10.1016/j.mejo.2010.01.011
26. M. A. A. Zadeh, H. Lari, L. Kharghanian, et al., J. Comput. Theor. Nanosci. **12**, 4358 (2015). https://doi.org/10.1166/jctn.2015.4366
27. M. Monajjemi, M. Khaleghian, N. Tadayonpour, et al., Int. J. Nanosci. **09**, 517 (2010). https://doi.org/10.1142/S0219581X10007071
28. F. Mollaamin, A. Ilkhani, N. Sakhaei, B. Bonsakhteh, A. Faridchehr, S. Tohidi, and M. Monajjemi, J. Comput. Theor. Nanosci. **12**, 3148 (2015). https://doi.org/10.1166/jctn.2015.4092
29. F. Mollaamin, M. Monajjemi, S. Salemi, and M. T. Baei, Fullerenes Nanotubes Carbon Nanostruct. **19**, 182 (2011). https://doi.org/10.1080/15363831003782932
30. F. Mollaamin and M. Monajjemi, J. Mol. Model. **29**, 119 (2023). https://doi.org/10.1007/s00894-023-05526-3
31. R. Dennington, T. A. Keith, and J. M. Millam, *GaussView, Version 6* (Semichem Inc., Shawnee Mission, KS, 2016).
32. M. J. Frisch, G. W. Trucks, H. B. Schlegel, G. E. Scuseria, M. A. Robb, J. R. Cheeseman, G. Scalmani, V. Barone, G. A. Petersson, H. Nakatsuji, X. Li, M. Caricato, A. V. Marenich, J. Bloino, B. G. Janesko, et al., *Gaussian 16, Revision C.01* (Gaussian Inc., Wallingford CT, 2016).
33. A. Bilić, J. R. Reimers, and N. S. Hush, J. Phys. Chem. B **106**, 6740 (2002). https://doi.org/10.1021/jp020590i
34. W. Malone and A. Kara, Surf. Sci. **693**, 121525 (2020). https://doi.org/10.1016/j.susc.2019.121525
35. M. Monajjemi, F. Mollaamin, M. R. Gholami, H. Yoosbashizadeh, S. K. Sadrnezhad, and H. Passdar, Main Group Met. Chem. **26**, 349 (2003).
36. F. Mollaamin and M. Monajjemi, Clean Technol. **5**, 403 (2023). https://doi.org/10.3390/cleantechnol5010020
37. D. Mollenhauer, N. Gaston, E. Voloshina, and B. Paulus, J. Phys. Chem. C **117**, 4470 (2013). https://doi.org/10.1021/jp309625h
38. C. Isvoranu, B. Wang, E. Ataman, K. Schulte, J. Knudsen, J. N. Andersen, M.-L. Bocquet, and J. Schnadt, J. Phys. Chem. C **115**, 20201 (2011). https://doi.org/10.1021/jp204460g
39. F. Mollaamin, S. Shahriari, M. Monajjemi, et al., J. Cluster Sci. **34**, 1547–1562 (2022). https://doi.org/10.1007/s10876-022-02335-1
40. F. Mollaamin and M. Monajjemi, Mol. Simul. **49**, 365 (2023). https://doi.org/10.1080/08927022.2022.2159996
41. V. V. Dhayabaran, J. P. Merlin, et al., Ionics **10**, 288 (2004).
42. A. D. Becke, J. Chem. Phys. **98**, 5648 (1993).
43. C. Lee, W. Yang, and R. G. Parr, Phys. Rev. B **37**, 785 (1988).
44. K. Kim and K. D. Jordan, J. Phys. Chem. **98**, 10089 (1994). https://doi.org/10.1021/j100091a024
45. K. Xhanari and M. Finsgar, Arab. J. Chem. **12**, 4646 (2019). https://doi.org/10.1016/j.arabjc.2016.08.009

46. R. Winston Revie, *Uhlig's Corrosion Handbook,* 3rd ed. (Wiley, New York 2011).

47. J. R. Davis, *Corrosion of Aluminium and Aluminium Alloys* (ASM Int., Ohio, 1999).

48. P. J. Stephens, F. J. Devlin, C. F. Chabalowski, and M. J. Frisch, J. Phys. Chem. **98**, 11623 (1994). https://doi.org/10.1021/j100096a001

49. C. J. Cramer, *Essentials of Computational Chemistry: Theories and Models,* 2nd ed. (Wiley, New York, 2004).

50. A. D. Becke, Phys. Rev. A **38**, 3098 (1988).

51. R. Ditchfield, W. J. Hehre, and J. A. Pople, J. Chem. Phys. **54**, 724 (1971).

52. R. A. Fry, K. D. Kwon, S. Komarneni, J. D. Kubicki, and K. T. Mueller, Langmuir **22**, 9281 (2006).

53. M. Finnis, Prog. Mater. Sci. **52**, 133 (2007). https://doi.org/10.1016/j.pmatsci.2006.10.003

54. A. Tahan, F. Mollaamin, and M. Monajjemi, Russ. J. Phys. Chem. A **83**, 587 (2009). https://doi.org/10.1134/S003602440904013X

55. K. Bakhshi, F. Mollaamin, and M. Monajjemi, J. Comput. Theor. Nanosci. **8**, 763 (2011). https://doi.org/10.1166/jctn.2011.1750

56. M. Monajjemi, M. T. Baie, and F. Mollaamin, Russ. Chem. Bull. **59**, 886 (2010). https://doi.org/10.1007/s11172-010-0181-5

57. L. A. Girifalco and V. G. Weizer, Phys. Rev. **114**, 687 (1959). https://doi.org/10.1103/physrev.114.687

58. H. Heinz, R. A. Vaia, B. L. Farmer, and R. R. Naik, J. Phys. Chem. C **112**, 17281 (2008). https://doi.org/10.1021/jp801931d

59. Ch. Kittel, *Introduction to Solid State Physics,* 3rd ed. (Wiley, New York, 1968).

60. A. A. El-Shafei, S. A. Abd El-Maksoud, et al., Corros. Sci. **46**, 579 (2004).

61. J. Aihara, J. Phys. Chem. A **103**, 7487 (1999). https://doi.org/10.1021/jp990092i

62. R. M. Silverstein, G. C. Bassler, and T. C. Morrill, *Spectrometric Identification of Organic Compounds,* 5th ed. (Wiley, New York, 1981).